J Mater Sci (2006) 41:5088–5098
DOI 10.1007/s10853-006-0442-8

Wetting of Group IV diborides by liquid metals

A. Passerone · M. L. Muolo · D. Passerone

Received: 30 September 2005 / Accepted: 15 February 2006 / Published online: 18 July 2006

Abstract The possibility to exploit the peculiar characteristics of transition elements diboride ceramics—a class of promising materials for high temperature and highly aggressive applications—often depends to a great extent on the ability to join the ceramic parts one to the other or to special metallic alloys. Therefore, the knowledge of wettability, interfacial tensions and interfacial reactions is mandatory to optimise the joining processes. Data on the wettability and the interfacial features of different metal–ceramic systems, particularly of (Ti,Zr,Hf)B_2 in contact with liquid non-reactive metals Cu, Ag, Au and their alloys, are reported and critically discussed, beginning with the pioneering work made in European eastern countries in the 70s up to the most recent published and new data. Moreover, interfacial energetics at the atomistic level is being increasingly investigated by means of sophisticated modelling techniques such as pseudopotential-based Density Functional Theory (DFT). These approaches will be presented, referred to non-oxide metal–ceramic systems. Given the complexity of ab initio calculations, the study is limited to the *ideal work of separation*, i.e. with plastic and diffusional degrees of freedom suppressed. Nevertheless, it is shown that the results on the specific transition borides-molten metal systems can be used to interpret the wetting behaviour and the adsorption/reaction interfacial phenomena involved.

A. Passerone (✉) · M. L. Muolo
Inst. for Energetics and Interphases—IENI CNR,
via de Marini, 6, 16149 Genova, Italy
e-mail: a.passerone@ge.ieni.cnr.it

D. Passerone
Inst. Organic Chem., Univ. Zurich, 8057 Zurich, Switzerland
e-mail: passero@oci.unizh.ch

Introduction

Non-oxide ceramics, such as carbides, nitrides and borides represent one of the fastest growing classes of new advanced materials to be considered and pursued by today's industries. The economic and technological significance of using these ceramics to improve present material structures and designs is now well documented. Transition metals ceramic diborides, such as titanium, hafnium and zirconium diborides, are members of a family of materials with extremely high melting temperatures, high thermal and electrical conductivity, excellent thermal shock resistance, high hardness and chemical inertness. These compounds, also referred to as Ultra High Temperature Ceramics (UHTCs), constitute a class of promising materials for use in high performance applications, where high temperatures, high thermal fluxes, severe surface stresses are involved. These conditions are met in the design of sharp edges on re-entry vehicles, thermal insulations in combustion chambers, special inserts in advanced brakes, cutting tools and plasma arc electrodes [1].

Since the mid-70's, large experimental efforts have been directed at resolving problems related to the processing aspects of metal/ceramic systems. Unfortunately, before a firm and thorough understanding of the effects of dissimilar interfaces on the processing and properties of these materials had been reached, interest in fundamental aspects was replaced by the need to

develop such metal/ceramic components for specific engineering applications. Research and development activity quickly moved to and have since led to great advancements. However, questions concerning the effects of interfaces have persisted and have caused uncertainties on the future development of these materials.

Indeed, the possibility to exploit the peculiar characteristics of these ceramic materials often depends to a great extent on the ability to join the ceramic parts one to the other or to special metallic alloys by means of diffusion bonding or brazing techniques. In this last case, the behaviour of the metal–ceramic joint is ruled by the chemical and physical properties of the interface, thus the knowledge of the interfacial energetics, that is of interfacial tensions, interfacial reactions and wettability is mandatory for understanding what happens at the liquid metal–ceramic interface during the joining processes.

Pure metals, in general, do not wet ceramic materials; therefore many efforts have been made to improve wetting in these metal–ceramic systems [2]. Two ways are widely used: one is to modify the ceramic surface by some specific coatings, in order to let the braze metals spread on this new surface, and the other way is to add reactive elements to the braze, which can form intermediate products at the interface more readily wetted by the liquid alloy. For example, the addition of Ti to Ag or Cu alloys involves the formation of Ti compounds (TiO, TiC or TiN on oxides, carbides and nitrides, respectively) at the metal–ceramic interface, which, due to their more ''metallic'' character, are wetted better than the underlying ceramic. Active metals additions can also work through an adsorption process, where the additional element accumulates at the solid–liquid interface lowering the interfacial energy, and, as a consequence, the contact angle affecting also the spreading kinetics [3–5].

As shown in the following, wetting experiments performed in the past years suffer from a large scatter of data. In the specific case of diborides the reasons for this can be attributed to different factors: firstly, the chemical composition and the surface structure of the solid specimens are hardly specified. Indeed, all materials studied up to now were obtained by various sintering techniques. Due to the high melting point and high vapour pressure of Ti-, Zr- and Hf-borides, the main technological barrier to the production of these materials is the sintering stage. Relatively high densities are achieved by pressure-assisted sintering procedures at temperatures approaching or even reaching higher than 2100–2300 °C. Generally the final microstructures are coarse and an amount of residual porosity is present, because the matter transfer active at these temperatures takes place through evaporation/condensation rather than volume diffusion processes.

The most recent efforts of the research and development activities on UHTC are addressed to improve the fabrication procedures and the performance of these ceramics through different routes (use of sintering aids, of Hot Isostatic Pressing HIP and Spark Plasma Synthesis SPS) [6–12].

Even so, high densification can hardly be obtained, unless specific sintering aids are used. However, sintering aids modify not only the ceramic structure, but can also form new phases, grain-boundary precipitates and new solid solutions: in all cases they change the nature of the ceramic body, so that the contact angle measurements should be referred to the new system, which is often hard to characterise or to reproduce [13]. These systems are very complex so that the study and understanding of the phenomena governing the interaction with metals is furthermore difficult and needs the involvement of multidisciplinary approaches. If sintering aids are not used, the resulting high surface porosity enhances the surface roughness to values, which may lead to meaningless contact angles (it should be remembered that a roughness $R \ll 0.1\ \mu$m should always be used [14]).

Moreover, in wetting experiments a third ''component'', besides the solid and the liquid phases, plays a major role: the surrounding atmosphere. Indeed, one of the most common sources of scatter among reported contact angle data, comes from the contamination of the liquid phase by active gases like oxygen. Oxygen transport phenomena related to the modification of liquid surface tension, solid–liquid interfacial tension and contact angles have been thoroughly studied in recent years [15–21]. One of the most important results is that, on top of the classical thermodynamic approach, dynamic transport processes must be taken into account, which show how, in many cases, the combined effects of metal atoms and sub-oxides evaporation can allow experiments to be carried out in ''clean'' conditions of the liquid metal surface even if equilibrium thermodynamics should foresee metal oxidation [15]. On the other hand, once they reach the liquid surface, active gases diffuse through the liquid phase and can reach the solid–liquid interface modifying its energetics by adsorption and/or formation of new phases.

Taken into account the great number of different parameters and factors affecting the properties of metal/ceramic interfaces, new specific models have to be developed for these kinds of systems. Such models have to be supported by experimental results obtained

with characterised-high purity materials in a controlled furnace environment.

Transition metal borides properties

Physical properties

The main physical properties of the transition metal borides are reported in Table 1. The first point to be underlined is that a large scatter exists in the data reported by various authors for these materials. Even for the melting temperature the agreement is very poor: this can be understood considering its extremely high value and the connected difficulties in measuring it. Moreover, another important source of uncertainty, for all measurements, is the poor definition of the purity of the specimens examined, their lack of compactness due to the sintering procedures, etc. In the authors' knowledge, only a few studies exist, and from only one laboratory [36], where measurements have been reported on single crystal specimens, and in this case, a low melting temperature for TiB_2 (2790 °C) was also reported [37].

These diborides are very stable, as shown by their negative free energy of formation, and have high stiffness and are metallic conductors with room temperature resistivities similar to those of their parent metals. Moreover, their thermal conductivity is high: this property has a relevant impact in the design of thermal protection barriers which make use of them to exploit their high melting point, stiffness and surface hardness.

Another important property is the thermal expansion coefficient. In a non-recent thorough study [38], also confirmed by recent results [39], this quantity (Table 2) has been evaluated as a function of temperature, thus giving the opportunity to design properly metal–ceramic joints.

Reactivity—oxidation properties

Transition metals diborides are very reactive towards oxygen and carbon monoxide as shown, from a thermodynamic point of view, in Table 3 in the case of HfB_2.

Indeed, the detailed knowledge of the thermodynamics and kinetics of these interactions is mandatory to define the correct working conditions for the evaluation of metal/ceramic interactions, in particular to give the correct interpretation for the results of wetting experiments. The results of Fig. 1 show that the three diborides are thermodynamically stable only at very low oxygen partial pressures. However, the oxidation

Table 1 Physical properties of transition metal diborides

Parameter	TiB_2	Ref	ZrB_2	Ref	HfB_2	Ref
Density [g/cm^3]	4.53	[22]	6.09	[22]	11.2	[22]
Melting point [°C]	3225	[23]	3220	[24]	3377	[25]
		[24]	3245	[26]	3380	[24]
Free energy of formation [kJ/mol]	−355 (RT)	[23]	−318.5 (RT)	[27]	−325.5 (RT)	[28]
	−307 (1000 K)	[23]	−307.3 (1000 K)	[27]	−320 (1000 K)	[28]
Heat of formation [kJ/mol]	−315	[23]	−331	[27]	−328	[29]
μHardness [GPa]	33	[30]	29.4	[31]	31.4	[31]
Young mod. [GPa]	224	[32]	490	[33]	450 (RT)	[34]
					330 (1000 °C)	
Electrical resistivity [$\mu\Omega$ cm]	20.4 (RT)	[26]	7.8 (RT)	[26]	10.6 (RT)	[22]
	56 (1000 °C)		17 (1000 °C)		45.8 (1000 °C)	
Thermal conductivity [W/(m K)]	64 (RT)	[22]	58 (RT)	[22]	83 (RT)	[34]
			23–25 (RT)	[35]	73 (800 °C)	

Table 2 Lattice constants and thermal expansion coefficients as a function of temperature for TiB_2, ZrB_2 and HfB_2 [38]

	Lattice constants [Å] vs. T [K^{-1}]	Linear thermal exp. coeff. vs. T [K^{-1}]	Average th. ex. coeff. at 1000 K [10^6 K^{-1}]
TiB_2	$A_1 = 3.0244 + 1.447\ 10^{-5}T + 5.853\ 10^{-9}T^2$	$k_1 = 5.351\ 10^{-6} + 1.933\ 10^{-9}T$	$K = 8.2$
	$A_2 = 3.2213 + 2.348\ 10^{-5}T + 6.628\ 10^{-9}T^2$	$k_2 = 7.884\ 10^{-6} + 2.051\ 10^{-9}T$	
ZrB_2	$A_1 = 3.1637 + 1.391\ 10^{-5}T + 7.109\ 10^{-9}T^2$	$k_1 = 5.061\ 10^{-6} + 2.243\ 10^{-9}T$	$K = 7.3$
	$A_2 = 3.5259 + 1.651\ 10^{-5}T + 7.386\ 10^{-9}T^2$	$k_2 = 5.298\ 10^{-6} + 2.091\ 10^{-9}T$	
HfB_2	$A_1 = 3.1380 + 1.168\ 10^{-5}T + 7.786\ 10^{-9}T^2$	$k_1 = 4.465\ 10^{-6} + 2.506\ 10^{-9}T$	$K = 7.18$
	$A_2 = 3.4716 + 1.726\ 10^{-5}T + 6.208\ 10^{-9}T^2$	$k_2 = 5.501\ 10^{-6} + 1.784\ 10^{-9}T$	
	A_1 = along the a-axis	$A_n = A_n(1 + k_n\Delta T)$	$K = (2k_1 + k_2)/3$
	A_2 = along the c-axis		

Table 3 Calculated thermodynamic values for reactions involving HfB_2 [ΔG and ΔH in (kJ/mol)] [29]

Reaction	$\Delta G_{1000\ °C}$	$\Delta H_{1000\ °C}$	$\Delta G_{1500\ °C}$	$\Delta H_{1500\ °C}$
$HfB_2 = Hf + 2B$	315	328	308	332
$HfB_2 + 3/2\ O_2 = Hf + B_2O_3$	−647	−901	−549	−889
$HfB_2 + O_2 = HfO_2 + 2B$	−569	−774	−491	−763
$HfB_2 + 5/2\ O_2 = HfO_2 + B_2O_3$ [40]	−1516	−1833	−1335	−1721
$HfB_2 + N_2 = Hf + 2BN$	38	−171	119	−166
$HfB_2 + 1/2C = Hf + 1/2B_4C$	278	296	270	298
$HfB_2 + C = HfC + 2B$	113	124	108	126
$HfB_2 + 1/2CO = 3/4Hf + 1/4HfO_2 + 1/2B_4C$	161	70	197	77
$HfB_2 + 2CO = HfO_2 + 2B + 2C$	−121	−546	43	−529
$HfB_2 + 2CO = HfO_2 + 0.5B_4C + 1.5C$	−330	−608	−25 1580 °C	−591
$HfB_2 + 3\ CO = Hf + B_2O_3 + 3C$	25	−561	252	−538
$HfB_2 + 3\ CO = HfC + B_2O_3 + 2C$	−176	−765	51	−743
$HfB_2 + 5CO = HfO_2 + B_2O_3 + 5C$	−410	−1435	−14 1518 °C	−1398
$HfB_2 + 1/2N_2 = Hf\ N + 2B$	61	−34	98	−28

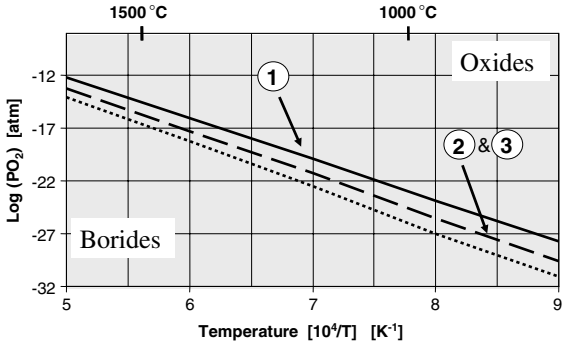

Fig. 1 Equilibrium oxygen pressure for the oxidation of (Ti,Zr,Hf) diborides (eqs. 1, 2, 3). The dotted line 3 represents the equilibrium B–O–B_2O_3 (l) system. (re-drawn from ref [40]).

$$TiB_2(s) + 5/2O_2(g) = TiO_2(s,l) + B_2O_3(l) \quad (1);$$

$$ZrB_2(s) + 5/2O_2(g) = ZrO_2(s,l) + B_2O_3(l) \quad (2);$$

$$HfB_2(s) + 5/2O_2(g) = HfO_2(s,l) + B_2O_3(l) \quad (3)$$

of these systems is strongly affected by kinetic factors: the oxide layer which forms at the surface slows down and even prevents further oxidation. This process leads to the possibility of high temperature applications of the diborides. It has been found [34] that in pure ZrB_2 the thickness of the oxidation layer increases with temperature (five times from RT to 1400 °C), confirming that boron oxide does not protect any more the bulk material.

Moreover, the role of boron should be taken into account: due to its small atomic radius, its diffusion to the ceramic surface is more pronounced than the diffusion of metal atoms. Thus, metal borates can form, at least at intermediate temperatures (around 1000 °C) improving the protective properties of the scales. At higher temperatures (>1100 °C), the relatively high vapour pressure of boron oxides becomes significant and will lead to the depletion of the boride phase, even if some residual 10% can be found in the oxidised scale [34]. This fact, bringing the surface to a sub-stoichiometric condition, can affect strongly the wettability characteristics of the ceramic piece, as shown in recent studies on carbides and nitrides systems [41–44].

Recent studies on the wetting kinetics of TiB_2 by Al [45] and on the influence of TiB_2 oxidation [46], reveal that the wetting kinetics of titanium boride, is highly dependent on the complex of surface reactions, leading to the elimination of B_2O_3 (liquid) layers by high temperature vaporisation. The following reduction of the underlying metal oxides through interactions with the molten metal leads to new equilibrium wetting configurations.

Wetting

Experimental studies of the energetics of the liquid metal–ceramic interfaces performed in the years 1950–1980, highlight major tendencies classifying ceramic–metal couples in ''wetting systems'' ($\theta < 90°$) and ''non-wetting systems'' ($\theta > 90°$). Unfortunately, for technological reasons, these experiments were performed using sintered polycrystalline ceramics. As already mentioned, the impurities in these materials, their surface roughness and the low quality of furnace atmospheres gave rise to a wide dispersion in values, thus, to a dispersion in the Work of Adhesion values (W_{ad}) as much as one or two orders of magnitude.

In the 70's a large amount of work was done, mainly in Ukraine, on the high-temperature wettability, reactivity (and oxidation) of transition metal borides. In an extensive study of wetting of Group IV–VI metal diborides [47], it was found that non-transition metals do not wet (contact angles > 90°) transition metals diborides, except Si which forms contact angles lower than 20° and Al, which spreads on the diborides at $T > 1300$ °C (Table 4). In their study, these authors report contact angle data on 46 systems. However, they point out that these same data are not sufficiently systematic, thus insufficient to draw general

Table 4 Contact angles (literature values [47]) of different metals on TiB_2, ZrB_2 and HfB_2

Boride	Metal	Contact angle	Temp. °C	Medium
TiB_2 [48]	Ag	126	1100	He
TiB_2 [48]	Ag	91	1600	He
TiB_2 [49]	Ni	38.5	1480	He
TiB_2 [50]	Ni	0	1500	Vacuum
TiB_2 [49]	Cu	158–154	1100–1500	Ar
TiB_2	Cu	135–132	1100–1300	Ar
TiB_2	Ga	115	800	Vacuum
TiB_2	In	124	300–500	Ar
TiB_2	Si	15	1500	Ar
TiB_2	Sn	114	250	Ar
TiB_2	Pb	106	350–800	Ar
TiB_2	Bi	141	320	Ar
TiB_2	Al	140–38	900–1250	Vacuum
ZrB_2 [50]	Fe	55	1550	Vacuum
ZrB_2 [50]	Co	39	1500	Vacuum
ZrB_2 [50]	Ni	42	1500	Vacuum
ZrB_2 [48]	Ag	114	1100	He
ZrB_2 [48]	Ag	70	1600	He
ZrB_2	Ga	127	800	Vacuum
ZrB_2	In	114	300–500	Ar
ZrB_2	Al	106–60	900–1250	Vacuum
ZrB_2	Ge	102	1000	Ar
ZrB_2	Sn	101	250–600	Ar
HfB_2	In	114	300–500	Vacuum
HfB_2	Ge	140	1000–1100	Vacuum
HfB_2	Al	134–60	900–1250	Vacuum

conclusions. All the boride specimens were prepared by hot pressing, and a porosity of 4–6% was reported. The general trend has been discussed in terms of electronic structure of both the borides and of the molten metal: in particular, the good wetting of Si and Al has been attributed to the fact that Si and Al are electron donors towards boron, i.e. with a higher chemical affinity for it.

The same authors [47] found that the diborides of group IV metals are more ''inert'' in contact with liquid Fe, Ni and Co (show larger contact angles) (Table 5) than those of V and VI groups, which show very low contact angles often going to complete spreading [51].

A remarkable result, also shown in Table 5, is the fact that the gaseous environment affects very strongly the wetting processes. Moreover, chemical reactions occur in these systems, especially under argon gas, which is not able to supply sufficiently reducing conditions: the angles given in Table 5 refer to the contact angle between the pure liquid metal and the diboride just after melting: these values are considered by the authors as the ''true'' metal-boride contact angles.

However, after a few seconds the contact angles decrease, reaching low values (for TiB_2: $\theta = 42°$ for Fe, $\theta = 26°$ for Ni and $\theta = 18°$ for Co in argon) due to interfacial reactions/dissolution and then to the change in composition of the solid–liquid interface. Results on

Table 5 ''Initial'' contact angles of Iron group metals on (IV, V, VI)-group borides [51].

Boride	Metal	Contact angle		Temp. °C
		Vacuum	Argon	
TiB_2	Fe	62	92	1550
ZrB_2	Fe	72	102	1550
HfB_2	Fe	100	98	1550
VB_2	Fe	17	–	1550
W_2B_5	Fe	0	0	1550
TiB_2	Ni	20	72	1480–1600
ZrB_2	Ni	65	78	1480–1600
HfB_2	Ni	99	98	1480–1600
VB_2	Ni	0	0	1450
W_2B_5	Ni	4	–	1450
TiB_2	Co	20	64	1500–1600
ZrB_2	Co	63	81	1500–1600
HfB_2	–	–	–	
VB_2	Co	0	0	1500
W_2B_5	Co	19	94	1500

the wettability of some mono- and diborides by Ni and Cu are also reported [52] confirming that the wettability increases with increasing the atomic number of the metal in the boride, while the liquid transition metals show a better wetting behaviour than non-transition metals. Monoborides are wetted much better. A correlation has been observed between wettability and resistivity (decreasing θ with increasing ρ) as well as with the heat of formation of the different borides. In particular, in another study [53] and in agreement with the results of Table 4, Ag has been found to wet increasingly well TiB_2 and ZrB_2, the contact angle decreasing from 125° for TiB_2 and 115° for ZrB_2 at 1100 °C to 92° and 74°, respectively, at 1600 °C.

Further work on the same systems has clearly shown that the contact angle of Ni alloys containing from 0.7 to 7.0%C or 0.7 to 24.7%Cr increased steadily in the series $TiB_2 < ZrB_2 < HfB_2$. In particular, it reached 140° at 4%C [54]. Aluminium was found to wet TiB_2, with contact angles going from 90 at 700 °C to 60 at 840 °C [55] under a vacuum. However, the liquid phase should have been oxidised, as shown by the reported low value of the Al surface tension at the melting point ($\gamma = 760$ mN/m).

Recent experimental results

More recent results on the wettability of group IV metal diborides are related to a renewed interest in these materials for advanced high temperature applications. Wetting of TiB_2 by molten Ni in relation to the development of cutting tools has also been studied [56]. Interfacial reactions have been found, with the formation of a liquid phase starting at 1310 °C, but

neither quantitative data on contact angles nor on interfacial energies are reported.

Other studies, where wettability problems were one of the key factors, discuss the influence of contact angles on, e.g. infiltration of TiB_2 and ZrB_2 powders, making reference to old contact angle data [57].

In the recent years, our Team has undertaken a systematic study, by the sessile-drop technique, of wettability, reactivity and interfacial properties of Group IV diborides, both from the basic (wettability, interfacial tension) and the application (joining) points of view [58–62].

A series of wetting results is presented in Table 6 for Ti, Zr and Hf diborides in contact with liquid Ag, Cu and Au. The experiments have been conducted using the sessile-drop technique in conjunction with the specially designed ASTRA© image analysis software which allows real time surface tension and contact angle data to be obtained during each experimental run [63, 64]. An especially designed furnace has been used which can reach 1600 °C. It is made of two concentric, horizontal, alumina tubes connected to a high vacuum line. Between the two tubes a constant flux of argon guarantees that even in the higher temperature range oxygen does not diffuse inside the experimental chamber. The pressure inside the inner tube can be kept below 10^{-4} Pa by a turbomolecular pump; alternatively, controlled atmospheres can be introduced inside the working chamber, up to 10^5 Pa, whereby its oxygen content is continuously monitored by solid state oxygen sensors at the inlet and at the outlet. Zirconium and hafnium diborides, sintered by ISTEC-CNR [9, 10] and U.C. Davies [65, 66] have been used in form of plates 12 × 12 × 2 mm. They have been polished down to a surface roughness Ra = 0.02 μm, carefully cleaned and then used for the sessile drop tests, whereas the metals have been mechanically cleaned and put on the top of the ceramic substrate in the form of small cylinders (< 1 g).

Table 6 Contact angles (θ) at $T = 1.05T_{melting}$ on IV group transition metals diborides

Metal *Ceramic*	Cu	Ag	Au	Sintering technique
TiB_2	91			HIP
ZrB_2			→ 0	SPS
	80	153	34	HIP
HfB_2	47	130	98	SPS

The experiments have been performed under a vacuum better than 10^{-4} Pa. In addition, a zirconium foil has been wrapped around the specimen in the form of a semi-cylinder as a getter (Muolo ML, Passerone A Submitted for publication) to keep the oxygen partial pressure low enough (10^{-27} Pa at 1100 °C).

These tests have shown, somewhat at variance with previous findings, that gold wets Zr boride much better than silver and copper. On the contrary, copper shows the lowest contact angle on HfB_2. In general, kinetics exists, leading to a stationary situation only after a long time (30–60 min) (Fig. 2).

This means that interactions should occur at the interface, most probably due to the reduction or evaporation of surface oxides as discussed in the previous paragraph, or to the dissolution of titanium and boron into the liquid metal, as suggested by recent SIMS measurements. In particular, dissolved boron should segregate to the liquid metal surface, with a relevant surfactant action. Surface tension measurements and calculations are under way to substantiate this hypothesis.

Moreover, gold and copper not only wet quite well the ZrB_2 and HfB_2 surfaces, respectively, but also can penetrate between the solid grains, as shown in Fig. 3. In the particular case of the Au/HfB_2 specimens, sintered by SPS with lower density, complete infiltration occurred.

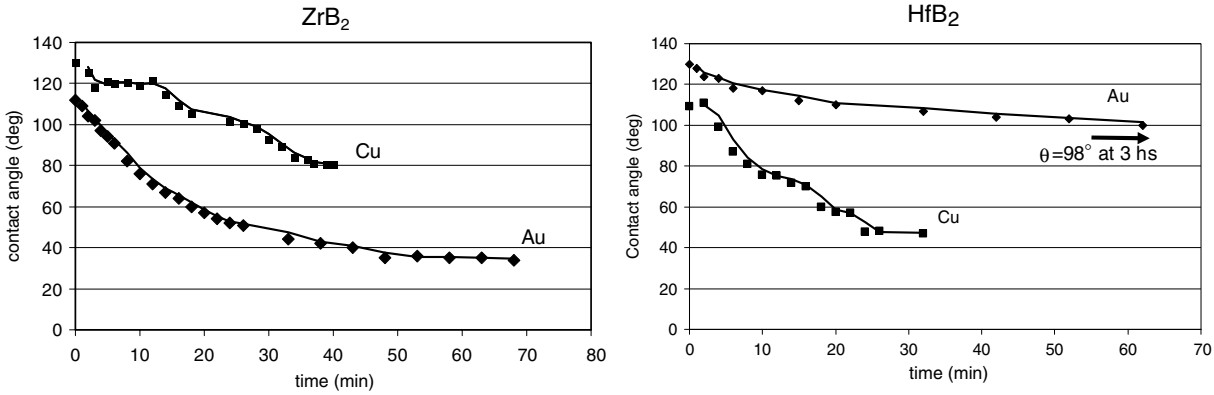

Fig. 2 Kinetics of spreading of Au and Cu on ZrB_2 and HfB_2 at 1323 K

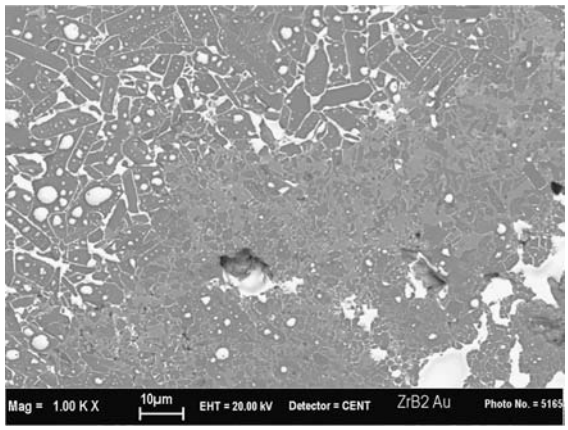

Fig. 3 Au penetration between ZrB_2 grains (upper left corner). In the presence of ZrO_2 grains (central part) no wetting/penetration occurs

As already discussed, the overall quality of the sintered borides, due to the high difficulties in the process, is not very high, mainly from the density and the compositional points of view. Indeed, especially in the case of Zr- and Hf-diborides, holes in the surface are commonly found (grains undermined in the polishing stage) together with oxide grains. In the case of gold, it was possible to show strong wetting differences between boride and oxide grains (Fig. 3). Moreover, small Au drops have been found on top of single boride grains, which allow an evaluation of the ''true'' contact angle on stoichiometric and ''smooth'' ZrB_2 surface. Assuming the solidification does not alter significantly the contact angle, its value was measured, in this case, in the range $\theta = 35–40°$, very close to the ''macroscopic'' angle measured at the experimental temperature.

Another series of experiments was aimed at elucidating the role of the addition of active metal elements on the wetting process of ZrB_2.

As shown in Fig. 4, while Ag does not show any contact angle evolution, a sharp decrease in contact angle is obtained by adding an ''active'' element, Ti, Zr or Hf, to the molten Ag matrix. However, the extent of this effect is different for the various metals. Zr seems to be the most effective in promoting wettability of the pure boride. The different spreading curves cannot be superimposed because the initial time does not represent specimens in the same physico-chemical conditions. Indeed, the melting and homogenisation time is not the same in all runs: on the contrary, once the active element is ''available'' in the liquid alloy, the spreading curves take on their full significance and can be compared to each other.

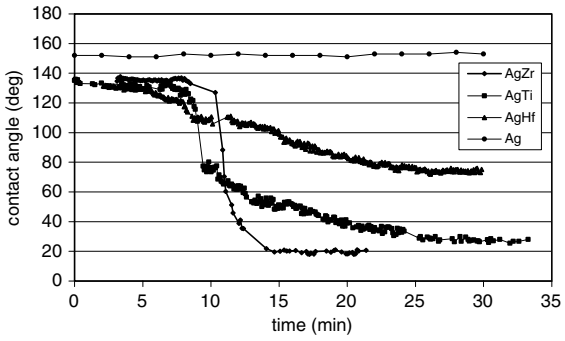

Fig. 4 Kinetics of spreading of different Ag–X alloys on ZrB_2 at $T = 1323$ K

In order to evaluate the energetics of the interaction phenomena at the experimental temperature, the Work of Adhesion can be computed using the Young–Dupré equation [2]: $W_{ad} = \gamma\ (1 + \cos\ \theta)$, provided the surface tension γ of the molten phase is known (Table 7). The pure metals surface tension values are from Ref. [67] (Ag, Cu) and from Ref. [68] (Ti, Zr and Hf), extrapolated to 1323 and 1423 K. Alloys surface tensions have been computed by the Quasi-Chemical Solution Model [69, 70] previously developed. As expected, the addition elements tend to rise the liquid alloy surface tension with respect to the matrix, confirming that the relevant phenomenon which promotes wetting is the segregation of the active element to the solid–liquid interface. This is also clearly shown by the high values of the Work of Adhesion obtained for the systems with Ti, Zr and Hf additions.

It is worth mentioning that the term ($\gamma\ \cos\theta$) represents the amount (''adhesion tension'') by which the solid surface tension is decreased by the solid–liquid interactions to give the interfacial tension value ($\gamma_{sv}-\gamma_{sl} = \gamma\ \cos\ \theta$). Provided the solid surface tension does not vary in the present case, when going from one liquid alloy to another (indeed, the same metal matrix is used, the additional elements have very low vapour pressures and the experimental conditions are the same), the values in the last column in Table 7 clearly show that Zr is much more efficient in promoting wetting and adsorbing/reacting at the interface.

Interfacial structure-modelling

As theoretical calculations of the Work of Adhesion are being increasingly attempted, a direct approach from first principles is still ''an unmanageable task'' [71]. Indeed, reviews [72] and dedicated papers [32, 73–77] are becoming available in literature, demonstrating a new line of approach aiming at a more quantitative comprehension of metal ceramic interfaces, based on first principles. In spite of difficulties to obtain sound

Table 7 Surface tension and contact angles for Ag–X alloys on pure ZrB_2

Metal/alloy (at%)	γ (mN/m) T = 1323 K	γ (mN/m) T = 1423 K	θ (T = 1323 K)	W_{ad} (mN/m) (T = 1323 K)	$\gamma \cos \theta$ mN/m
Cu		1272	$80_{1423\ K}$	$1493_{1423\ K}$	221
Au	1145	1095	34	2094	949
Ag	913	898	153	995	−813
Ag–Ti 2.4	931	916	27	1761	830
Ag–Zr 2.4	929	914	21	1796	867
Ag–Hf 2.4	933	918	$75_{1323\ K}$	$1175_{1323\ K}$	$242_{1323\ K}$
			$53_{1423\ K}$	$1471_{1423\ K}$	$553_{1423\ K}$

results from first principles, an ideal ''Work of Separation'' (i.e. with plastic deformation and diffusional degrees of freedom suppressed) can be evaluated by means of modelling techniques such as the density functional theory (DFT). Wetting of titanium carbides and nitrides has been analysed by this technique in the framework of the generalised gradient approximation [71]. In their remarkable study, the authors have been able to rationalise the relative contributions of metal–over Ti and metal–over carbon or nitrogen to the interfacial energy and then to contact angles. A general conclusion of this study is that the adhesion between the metal and ceramic phases can be thought as due to two kinds of chemical interactions across the interface: the metal–carbon (or nitrogen) and the metal–metal ones. The number (density) of each kind of bonds at the interface determines its final strength. In particular, it was inferred that, in the case of experimentally observed poor wetting, a good correlation is found with the metal–over Ti model interface. The transition to wetting can be related to a balanced mixture of metal–over Ti and metal–over carbon (or nitrogen) configurations. Wetting depends also on the orientation dependence of the interfacial energy. It was found that the most energetically favoured structures are the ones having the maximum total number of metal–carbon (or nitrogen) and metal–Ti bonds per metal atom. The work of separation in the series Ag, Cu and Au/TiC and/TiN, correlates well with the variations of the charge-density values at the interface with metal–carbon (or nitrogen) bonds. Moreover, the metal–TiC interfaces are stronger than the metal–TiN ones. This can be attributed to the more tightly bound electrons of N in TiN than the corresponding bonds in TiC, which in turn give rise to weaker metal/TiC interfaces (with respect to the metal/TiN ones).

In a similar study, devoted to the Ti/TiN system [77], it has been shown that the optimal structure (i.e. the one with the largest adhesion energy) is the one continuing the nitride crystal structure of the ceramic phase with the N-terminated surface: this configuration shows a calculated adhesion energy of about 7 J/m^2, about 4 J/m^2 larger than the Ti-terminated one. The Ti-terminated surface results with a mixed strong metallic and weak covalent character, while the N-terminated interface is dominated by polar covalent bonds, similar to the Ti/TiC interfaces.

Recently, we begun performing a first-principles DFT study to investigate similar properties for the interfaces between ZrB_2 and the transition metals Ag and Au.

To this end, the ESPRESSO package [78] and the Perdew–Burke–Ernzerhof (PBE) generalised gradient approximation have been used.

To model the interface, periodically repeated supercells with 4 or 5 layers of metal and 4.5 cells for ZrB_2 have been used, by studying, separately, the interface of the metal with a Zr-terminated slab and a B-terminated slab. Each layer is composed of 4 (Zr, Ag/Au) or 8 (B) atoms.

Given the relatively small mismatch of the lattice constants, and the hexagonal structure of ZrB_2 compared to the fcc structure of the metal, an interface between two (111) faces has been chosen.

The lattice parameters of ZrB_2 (Table 8) are kept like those in unstrained bulk. The in-plane lattice constant of the metal phase is adjusted to give a commensurate structure with the ZrB_2 slab. The metal

Table 8 Crystal structure of TiB_2, ZrB_2 and HfB_2

	Structure type C32	Lattice parameters A axis [nm]	Lattice parameters C axis [nm]	Ref.
TiB_2	Hexagonal lattice,	0.3038	0.3228	[79]
ZrB_2	with HCP Ti layers	0.3170	0.3533	[79]
	alternative with	0.31685	0.35295	[36]
HfB_2	graphite-like B layers	0.3139	0.3473	[79]
		0.3142	0.3475	[36]

out-of-plane lattice constant is optimised in bulk calculations to minimise the bulk strain introduced by the in-plane lattice distortion.

To describe electron–core interactions, ''ultrasoft'' pseudopotentials for Au, Ag, Zr, and B have been used, with non-linear core corrections. The pseudopotentials have been tested for the bulk lattice constant obtaining satisfactory results for all species.

The calculations are performed by relaxing the position of all atoms until residual forces are less than 0.03 eV $Å^{-1}$ (0.5 pN). All of the relevant details and specific results will be presented in a paper currently under preparation.

The first value extracted from calculations is the work of separation, defined as [71]:

$$W_{sep} = (E_{sl1} + E_{sl2} - E_{int})/2A,$$

where E_{int} is the total energy of the supercell with the interface system, E_{sl1} and E_{sl2} are the total energies of the same supercell, when one of the slabs is kept and the other one is replaced by vacuum, and A is the interface area within one supercell (there are two identical interfaces per supercell). To calculate the work of separation for the unrelaxed and relaxed interface structures, the relaxed values of all quantities have been used. The following preliminary values have been found: 2.03 J/m^2 for the B-terminated surface, in the case of Ag, 2.47 J/m^2 in the case of Ag and of 3.725 J/m^2 for Au for the Zr-terminated surface (all results with four k-points). These results indicate that the interface between Au and ZrB_2 (with Zr termination) is energetically more stable than the one involving silver. It should be noted that this kind of calculation provides information about the *energy part* of the free energy (at $T = 0$ K), neglecting entropic contributions that are of course present at higher temperatures. Nevertheless, although the behaviour of W_{sep} can give only qualitative conclusions about the work of adhesion, this trend can be confirmed by the recent experiments shown in Table 7.

For all the cases cited above the calculations have been repeated doubling the number of k-points in both lateral directions. When symmetry is kept into account, this corresponds to increasing the number of k-points from 4 to 10. No significant changes (less than 1%) have been found in the work of separation.

In another series of calculations the interface between Au and the Zr-terminated diboride surface has been evaluated, testing the possibility of another kind of relative displacement. In particular, the geometry of an interface where the gold atoms lie directly above the Zr ones (and not in the hollow sites proposed by the fcc structure) has been optimised, in order to investigate the possibility of more direct chemical bonding. Also in this case, both the interfacial distance and the overall geometry were fully optimised, yet the work of adhesion was found to be of 2.62 J/m^2, suggesting a less stable configuration.

Finally, a charge density plot at the interface between Au and ZrB_2 in the fcc-like interface case, with Zr-termination is reported (Fig. 5). The units are in electrons/$Bohr^3$, and the plane shown is a yz plane. Starting at the bottom, a B_2 layer is shown, followed by a Zr, another B_2, a Zr, and then three Au layers. Some bonding is present between Au and Zr, and the kind of bonding seems very similar to the one observed within the gold section of the slab, where the bonding is essentially metallic. Further investigation is in progress to draw conclusions about the microscopic character of the interfacial adhesion.

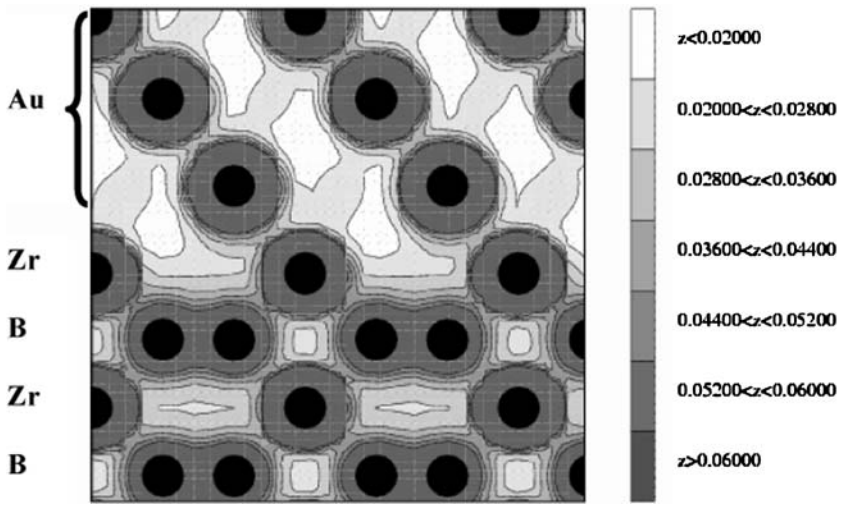

Fig. 5 Charge density plot at the interface between Au and ZrB_2 in the fcc-like interface case, with Zr-termination. The units are in electrons/$Bohr^3$, and the plane shown is a yz plane (1 Bohr = 0.0529 nm)

Conclusions

The peculiar physical, chemical and mechanical properties of transition metal diborides make them the ideal material for applications where extreme conditions are encountered, namely very high temperatures, high stresses, high surface mechanical and thermal loads.

Possible applications foresee the brazing of borides elements to each other or to supporting metal structures. Thus, their interactions with molten filler alloys should be studied, and particularly their wettability characteristics.

A thorough research covering the last 50 years has shown that wettability data exist but with a very large scatter among the data and insufficient definition of the experimental conditions, mainly due to the fact that macroscopic systems are often not homogeneous, porous etc. Moreover, the environmental conditions should be strictly defined especially in terms of oxygen partial pressures.

Recent results have shown that ''pure'' Group IV transition metal borides are not wetted by pure Ag, whereas Au and Cu not only reach low contact angles on the borides surfaces, but can also ''percolate'' along the boride grain boundaries. When the sintered boride density is not very high, impregnation of the solid mass can occur.

However, the addition of active metals such as Ti, Zr or Hf to pure Ag, leads to very good wetting properties. Similarly, the same effect can be obtained using ad hoc sintering aids, like Ni [58, 62].

Nevertheless, it appears clear that additional studies are needed on ''pure'' metal borides, in order to arrive at reliable data on wetting and interfacial structures which could be attributed to the real liquid metal–diboride system. To this end, experiments on a ''micro'' scale and the use of diboride monocrystals should help. At the same time, a theoretical approach is possible, which makes use of advanced modelling techniques, like molecular dynamics and dynamic functional theory (DFT). Preliminary results have been presented in a very good agreement with the most reliable experimental data.

We are aware that there is still a long way to go in building the bridge between high-temperature thermodynamically relevant experimental results and microscopic, computer-driven theoretical insight.

Nevertheless, given these preliminary findings, we find the strategy promising. Little to nothing is known about the nature of the interfacial bonding in the discussed systems, or on the effect of the microscopic composition and structure on the macroscopic and technologically relevant properties. This approach needs indeed to be seen within the following perspectives:

- Validation of the results (increased cutoff, number of *k*-points, number of atoms per layer)
- Reduction of the lattice spacing mismatch using different relative orientations at the interface
- Test with other borides
- Estimation of the interfacial free energy for all systems
- Substitution of selected interfacial atoms with other elements (e.g. Ti)
- Connection with finite temperature properties and experimental data (contact angle, work of adhesion)
- Tailoring and production of novel materials upon suggestions coming from DFT calculations.

Acknowledgements The authors wish to express their thanks to Dr. A. Bellosi (ISTEC-CNR) for supplying most of the HIP metal diboride specimens, and to Prof. Z. Munir (U.C. Davies) and to Dr. U. Anselmi-Taburini (IENI-Pv) who kindly supplied some explorative Hf-diboride specimens made by SPS. The contribution of Dr. G. Battilana and C. Bottino (IENI-Ge) (SEM and EDS analyses) is also gratefully acknowledged.

References

1. Weimer AM (ed) (1997) Carbide, nitride and boride materials: synthesis and processing. Chapman & Hall, New York
2. Eustathopoulos N, Nicholas MG, Drevet B (1999) Wettability at high temperature. UK Pergamon Materials Series, Elsevier Sci., Oxford
3. Saiz E, Tomsia AP (2004) Nature Mater 3:903
4. Gremillard L, Saiz E, Chevalier J, Tomsia AP (2004) Zeit Metallk, Mater Res Adv Tech 95:261
5. Saiz E, Tomsia AP, Saganuma K (2003) J Eur Ceram Soc 23:2787
6. Sciti D, Melandri C, Bellosi A (2004) Adv Eng Mater 6(9):775
7. Monteverde F, Bellosi A (2005) J Eur Ceram Soc 25:1025
8. Medri V, Balbo A, Monteverde F, Bellosi A (2005) Adv Eng Mater 7(3):159
9. Monteverde F, Bellosi A (2004) J Mater Res 19:3576
10. Monteverde F, Bellosi A (2004) Adv Eng Mater 6:331
11. Monteverde F, Bellosi A (2003) Adv Eng Mater 5:508
12. Monteverde F, Bellosi A, Guicciardi S (2003) Mater Sci Eng A 346:310
13. Saiz E, Tomsia AP, Cannon RM (2001) Acta Mater 44:159
14. Eustathopoulos N, Sobczak N, Passerone A, Nogi K (2005) J Mater Sci 40:2271
15. Arato E, Costa P, Ricci E (2005) J Mater Sci 40:2133
16. Ricci E, Ratto M, Arato E, Costa P, Passerone A (2000) ISIJ Int 40:139
17. Chatain D, Ghetta V, Fouletier J (1998) In: Tomsia AP (ed) Ceramic microstructure: control at the atomic level. New York, Plenure press, p. 349
18. Backhaus-Ricoult M (2000) Acta Mater 48:4365

19. Laurent V, Chatain D, Eustathoupoulos N (1988) Acta Met 36:1797
20. Castello P, Ricci E, Passerone A, Costa P (1994) J Mater Sci 29:6104
21. Ratto M, Ricci E, Arato E (2000) Crystal Growth 217:233
22. Samsonov GV, Vinitskii IM (1980) Handbook of refractory compounds. IFI-Plenum, New York
23. Ma X, Li C, Du Z, Zhang W (2004) J Alloys Comp 370:149
24. Massalski TB (ed) (1990) Binary alloy phase diagrams, 2nd edn. ASM, OH
25. Rogl P, Bittermann H (2000) J Solid State Chem 154:257
26. Rahman M, Wang CC, Chen W, Akbar SA (1995) J Am Ceram Soc 78:1380
27. Chase MW et al (1985) J Phys Chem Ref Data 14(suppl. 1):1
28. Nakae H, Yamamoto K, Sato K (1990) J Jpn Inst Met 54:839
29. Blum YD, Kleebe HJ (2004) J Mater Sci 39:6023
30. Ordan'yan SS, Unrod VI, Avgustinik AI (1975) Poroshkovaya Metallurgiya 9:40
31. Bsenko L, Lundström T (1974) J Less Common Met 34:273
32. Vajeeston P, Asokamani R (2000) V Nat Conf High Press Sci & Techn, Anna Univ. Chennai, India
33. Telle R, Sigl LS, Takagi K (2000) In: Riedel R (ed) Handbook of ceramic hard materials. Wiley-VCH, Weinheim, p. 803
34. Opeka MM, Talmy IG, Wuchina EJ, Zaykoski JA, Causey SJ (1999) J Eur Ceram Soc 19:2405
35. Mishra SK, Das S, Das SK, Ramachandrarao P (2000) J Mater Res 15:2499
36. Otani S, Korsukova MM, Mitsuhashi T (1998) J Crystal Growth 186:582
37. Otani S, Ishizawa Y (1994) J Crystal Growth 140:451
38. Lönnberg B (1988) J Less Common Met 141:145
39. Okamoto NL, Kusakari M, Tanaka K, Inui H, Yamaguchi M, Otani S (2003) J Appl Phys 93:88
40. Singh M, Wiedermeier H (1991) J Am Ceram Soc 74:724
41. Xiao P, Derby B (1996) Acta Mater 44:307
42. Muolo ML, Bassoli M, Wollein B, Lengauer W, Passerone A (2001) Trans JWRI 30:49
43. Kalogeropoulou S, van Deelen J, Eustathopoulos N, Le Guyadec F, Berardo M (2001) Trans JWRI 30:107
44. Froumin N, Frage N, Polak M, Dariel MP (2001) Trans JWRI 30:91
45. Weirauch DA, Krafick WJ, Ackart G, Ownby PD (2005) J Mater Sci 40:2301
46. Koh Y-H, Lee S-Y, Kim H-E (2001) J Am Ceram Soc 84:239
47. Samsonov GV, Panasyuk AD, Borovikova MS (1973) Poroshkovaya Metallurgiya 5:61
48. Ukov VP, Esin OA, Vatolin NA, Dubinin EL (1971) Phys Chem Interf Phen High Temp. Naukova Dumka, Kiev, p. 139
49. Eremenko VN, Naidich YUV (1959) J Neorg Chem 4:931
50. Kotsch H (1967) Neue Hütte 12:350
51. Samsonov GV, Panasyuk AD, Borovikova MS (1973) Poroshkovaya Metallurgiya 6:51
52. Tumanov VI, Gorbunov AE, Kondratenko GM (1970) Russian J Phys Chem 44:304
53. Ukov V, Esin OA, Vatolin HA et al (1971) Physical chemistry of surface phenomena at high temperature. Naukova Dunka, Kiev, Ukraina, p. 139
54. Samsonov GV, Panasyuk AD, Borovikova MS (1974) In: Eremenko VN, Naidich YuV (eds) Adgez. Rasplavov. Naukova Dumka, Kiev, Ukraina, p. 142
55. Rhee SK (1970) J Am Ceram Soc 53:386
56. Fenard E, Desmaison-Brut M, Joyeux T (2002) Euro ceramics VII. Trans Tech Publications Ltd, Zurich, Switzerland, p. 563
57. Kennedy AR, Wood JD, Wagner BM (2000) J Mater Sci 35:2909
58. Muolo ML, Ferrera E, Novakovic R, Passerone A (2003) Scripta Mater 48:191
59. Muolo ML, Ferrera E, Morbelli L, Zanotti C, Passerone A (2003) ESA SP-540:467
60. Passerone A, Muolo ML, Morbelli L, Ferrera E, Bassoli M, Bottino C (2003) ESA SP-521:295
61. Daolio S, Fabrizio M, Piccirillo C, Muolo ML, Passerone A, Bellosi A (2001) Rapid Comm Mass Spectr 15:1
62. Muolo ML, Ferrera E, Passerone A (2005) J Mater Sci 40:2295
63. Liggieri L, Passerone A (1989) High Temp Tech 7:82
64. Passerone A, Ricci E (1998) In: Moebius D, Miller R (eds) Drops and bubbles in interfacial research. Elsevier, Amsterdam, p. 475
65. Anselmi-Tamburini U, Munir ZA, Kodera Y, Imai T, Ohyanagi M (2005) J Am Ceram Soc 88:1382
66. Anselmi-Tamburini U, Garay JE, Munir ZA (2005) Mater Sci Eng A 407:24
67. Joud JC, Eustathopoulos N, Desré P (1972) CR Acad Sci Paris: Série C 274:549
68. Ishikawa T, Paradis PF, Itami T, Yoda S (2003) J Chem Phys 118:7912
69. Novakovic R, Ricci E, Muolo ML, Giuranno D, Passerone A (2003) Intermetallics 11:1301
70. Novakovic R, Muolo ML, Passerone A (2004) Surf Sci 549:281
71. Dudiy SV, Lundqvist B (2004) Phys Rev B 69:125421
72. Sinnot SB, Dickey EC (2003) Mater Sci Eng R 43:1
73. Swiler TP, Loehman RE (2000) Acta Mater 48:4419
74. Köstlmeier S, Elsässer C (2000) J Phys Conden Matter 12:1209
75. Dudiy S, Ph.D Thesis, Chalmers Univ. of Techn., Applied Phys. Rep. 2002–45, Göteborg Univ., Sweden
76. Han X, Zhang Y, Xu H (2003) J Comp Phys 25:968
77. Liu LM, Wang SQ, Ye HQ (2003) Surf Interf Anal 35:835
78. Baroni S, Dal Corso A, De Gironcoli S, Giannozzi P, Cavazzoni C, Ballabio G, Scandolo S, Chiarotti G, Focher P, Pasquarello A, Laasonen K, Trave A, Car R, Marzari N, Kokalj A. http://www.pwscf.org/
79. Vajeeston P, Ravindran P, Ravi C, Asokamani R (2001) Phys Rev B 63:045115